LA-UR- 08-7585

Approved for public release;
distribution is unlimited.

Title:	Quantitative Laser-Induced Breakdown Spectroscopy Data Using Peak Area Step-wise Regression Analysis: An Alternative Method for Interpretation of Mars Science Laboratory Results
Author(s):	Samuel M. Clegg Melinda D. Dyar Martha W. Schaefer Jonathan M. Tucker James E. Barefield Roger C. Wiens
Intended for:	Geophysical Research Letters

Los Alamos
NATIONAL LABORATORY
EST.1943

Form 836 (7/06)

Quantitative Laser-Induced Breakdown Spectroscopy Data Using Peak Area Step-wise Regression Analysis: An Alternative Method for Interpretation of Mars Science Laboratory Results

M. Darby Dyar[1], Martha W. Schaefer[2], Samuel M. Clegg[3], Jonathan M. Tucker[4], James E. Barefield II[3], and Roger C. Wiens[3]

[1]Department of Astronomy, Mount Holyoke College, South Hadley, Massachusetts, USA.

[2]Department of Geology and Geophysics, Louisiana State University, Baton Rouge, Louisiana, USA.

[3]Los Alamos National Laboratory, Los Alamos, New Mexico, USA.

[4]Department of Astronomy, Amherst College, Amherst, Massachusetts, USA.

Index terms: LIBS, laser-induced breakdown spectroscopy, calibration, Mars, ChemCam, matrix effects

Abstract. The ChemCam instrument on the Mars Science Laboratory (MSL) will include a laser-induced breakdown spectrometer (LIBS) to quantify major and minor elemental compositions. The traditional analytical chemistry approach to calibration curves for these data regresses a single diagnostic peak area against concentration for each element. This approach contrasts with a new multivariate method in which elemental concentrations are predicted by step-wise multiple regression analysis based on areas of a specific set of diagnostic peaks for each element. The method is tested on LIBS data from igneous and metamorphosed rocks. Between 4 and 13 partial regression coefficients are needed to describe each elemental abundance accurately (i.e., with a regression line of $R^2 > 0.9995$ for the relationship between predicted and measured elemental concentration) for all major and minor elements studied. Validation plots suggest that the method is limited at present by the small data set, and will work best for prediction of concentration when a wider variety of compositions and rock types has been analyzed.

1. Introduction

The ChemCam instrument selected for the Mars Science Laboratory (MSL) includes a Laser-Induced Breakdown Spectrometer (LIBS). The LIBS technique is related to conventional optical emission spectroscopy, in which the intensities of emission peaks diagnostic of individual

elements are related to concentration. However, LIBS spectra are sensitive to chemical matrix effects, which influence the ratio of a given emission line to the abundance of the element producing that line. The intensity of a given emission line may be affected by laser-to-sample coupling efficiency, the abundance of other neutral and ionized species within the plasma, collisional interactions within the plasma, and self absorption (see discussion in *Clegg et al.*, 2008 and citations therein). Atmospheric composition and pressure also significantly influence LIBS plasma intensity because the atmosphere is also broken down by the laser, producing excited atomic species that interact with the ablated surface material. All of these factors make extracting quantitative elemental concentrations of complex geochemical samples using LIBS a challenge.

Two existing strategies address these challenges. The traditional analytical chemistry approach to calibration relates elemental concentration to the area (or intensity) of a single diagnostic peak (e.g., *Buckley et al.*, 2000; *Fabre et al.*, 2002; *Anzano et al.*, 2006; *Thompson et al.*, 2006). More recently, *Clegg et al.* (2008) present a method for analyzing Mars-analog LIBS spectra using partial least squares analysis (PLS) of the intensity of all channels of each spectrum collected (see also *Fink et al.*, 2002; *Martin et al.*, 2005; *Bousquet et al.*, 2007). This method uses the statistical relationship between the LIBS data (the independent variables) and the elemental composition (dependent variables). The PLS method was tested on a challenging suite of igneous and metamorphic rocks with very promising results. Its strengths are that it does not presume to associate any given channel with any particular element and it appears to compensate for the chemical matrix effects.

In this paper, we test a new method of analyzing LIBS spectra with the potential to yield analytical results comparable to those produced by the *Clegg et al.* (2008) method. It is a derivative of the traditional approach in that it relates peak areas to concentrations. However, it uses *multiple peaks* for each element, such that elemental concentration is described by a multiple regression equation. For each element, step-wise multiple regression analysis is used to quantitatively select peaks with areas that correlate with concentration, so an optimized numerical calibration equation (of the form $Y = b_0 + b_1X_1 + b_2X_2 + b_3X_3 + \ldots + b_{n-1}X_{n-1} + b_nX_n$, where X = peak area and b is a partial regression coefficient) can be calculated. This technique represents an extension of the traditional approach of quantifying elemental abundances based on single peak areas that uses the more sophisticated possibilities available through multivariate statistical analysis. The goal of this paper is to describe Peak Area Step-wise Regression Analysis (PASRA), use it to analyze part of the same spectral data set employed by *Clegg et al.* (2008), and contrast it with the traditional analytical chemistry approach.

2. Experimental

2.1. Sample selection and Preparation

Samples for this study are the same as those used in the study of *Clegg et al.* (2008), which were analyzed for major and minor elements in the XRF lab at the University of Massachusetts (under the direction of Michael J. Rhodes) using their standard operating procedures (*Rhodes and Vollinger*, 2004). Rock types represent a range of common igneous compositions and also include a metamorphosed gabbro and basalt (petrogeneses are given in *Clegg et al.*, 2008). These particular samples were chosen because their broad range of compositions (Table 1) and rock types would create extended calibration curves for each element. Because the LIBS line intensities physically respond to the atomic fraction of a given element rather than its oxide weight percent, it was necessary to recalculate elemental analyses reported

in wt% oxides and parts per million into atomic fractions for subsequent regression analysis (see *Clegg et al.*, 2008 for more information).

2.2. Experimental Methods

Data acquisition is described in *Clegg et al.* (2008) and will only be briefly summarized here. Samples were powdered to <45 μm grain size and pressed into pellets. Experimental parameters for acquisition of spectra were selected to replicate those of the ChemCam LIBS instrument (*Maurice et al.*, 2007; *Wiens et al.*, 2007) as closely as possible; samples were run in a chamber filled with ~7 Torr CO_2 to simulate the martian surface atmosphere. A Spectra-Physics Indi Nd:YAG laser operating at 1064 nm, 10 Hz repetition rate, and a 10 ns pulse width was focused onto the samples. The laser energy was set to 17±1 mJ/pulse. The plasma emission was collected with a Questar Field Model Telescope with an 89 mm aperture that is smaller than the 110 mm telescope on ChemCam. The collected emission was directed into a 1 m, 300μm, 0.22NA, Ocean Optics Solarization Resistant fiber connected to one of three Ocean Optics HR2000 spectrometers covering 223.40 – 325.97 nm (UV), 381.86 – 471.03 nm (VIS) and 494.93 – 927.06 nm (VNIR). The spectral resolutions for the UV, VIS, and VNIR spectrometers are 0.1, 0.09 and 0.42 nm, respectively.

The spectrometer exposure time was set to 1 s in order to record the plasma emission for ten laser shots. The spectrometer software was set to average five of these exposures for each sample spot probed. Consequently, each probed spot represents 50 laser shots. Five different spots on each pressed pellet were sampled to account for any heterogeneity in these powdered samples.

2.3. Data Processing

An IDL (Interactive Data Language) routine was written for preprocessing and analysis of the LIBS spectra (*Schaefer et al.*, 2008). Each spectrum was normalized to its total integrated intensity to compensate for experimental fluctuations such as shot-to-shot changes in laser power and laser-to-sample coupling (cf. *Thompson et al.*, 2006 and *Clegg et al.*, 2008). Normalized spectra were then multiplied by a common scaling factor to make the normalized spectral intensities similar to the originally-recorded intensities. For each of the three detectors, this scaling factor is the double sum of the intensities over both the 2048 channels and five spectra, divided by five. The resultant spectra were the exact same as those used in the analysis of *Clegg et al.* (2008), though the latter study used only the intensity at each channel, which was directly input into the statistical analyses.

Because of the geometry of the crossed Czerny-Turner spectrometers, all three spectrometers used are spectrally non-linear, such that the wavelength spacing between channels is not consistent. Therefore, the entire spectral range is linearly interpolated to create a data set with the same number of channels as the initial file, but with the channels replaced by wavelength values with consistent spacings.

For background subtraction, an adaptation of the fit_background subroutine developed by Mark Rivers for the MCA analysis library (http://cars9.uchicago.edu/software/idl/mca_utility_routines.html#FIT_BACKGROUND) was used. This routine implements an enhanced version of the algorithm published by *Kajfosz and Kwiatek* (1987).

Peak characteristics can then be calculated using a subroutine based on the fit_peaks subroutine from the MCA analysis library (http://cars9.uchicago.edu/software/idl/mca_utility_routines.html#FIT_PEAKS). This routine can fit spectra to Gaussian, Lorentzian, or Voigt peaks (Gaussian for this study) and compare

them to a look-up table containing peak positions for all geologically-reasonable elements. Peak centroids and areas are saved to an ASCII file, and binned into wavelength increments for use in regression analyses.

3. Statistical Analyses

The traditional analytical chemistry approach to calibration uses the area of a single peak (or a ratioed, normalized peak area) that is highly correlated with the concentration for each specific element: the choice of which peak to use varies according to the matrix of the material being studied (Figure 1A). For geological samples with complex compositions and unknown matrix effects, peak choice is particularly important. To identify which peaks will be useful to predict concentration in our samples, we regressed the area in each bin (actually, a running sum of five adjacent 0.1 nm bins to accommodate changes in peak centroid with matrix, and peaks that fall barely in adjacent bins) against the concentration of each element. A best-fit linear regression line was calculated using measured atomic fraction as the dependent variable and the area of the five adjacent summed bins as the independent variable at each wavelength in 0.1 nm increments. The R^2 value (the proportion of the variation in the atomic fraction that is explained by the regression model) for that regression equation was plotted against wavelength (e.g., Figure 2 top for Ca, and Figure 3 for Zr, K, and Fe). For some elements (e.g., K), there are only a few conspicuous wavelengths that predict concentration with $R^2>0.5$, and some of these lines may well be emissions from other elements (such as Ca). These correlations with other elements are important to understanding how the technique compensates for matrix effects. For other elements (especially transition metals) such as Fe (Figure 3), there are many bins with areas that correlate strongly to concentration (e.g., $R^2>0.7$). Concentration can thus be qualitatively predicted by analyzing an individual peak or by using multiple major peaks, analyzed individually, to determine multiple predicted concentrations that can then be averaged.

For any of these elements at any wavelength, the Y intercept of the regression equation (predicted concentration) calculated on the basis of a single peak centroid is usually non-zero because matrix effects are playing a role in perturbing the relationship between emission and concentration (Figure 2, bottom). This is apparent in Figure 1 (top), which shows the regression line calculated between the measured atomic fraction of Ca and the atomic fraction predicted by a regression based on the "best" wavelength bin at 422.8 nm.

Alternatively, statistical parameters can be used to select multiple peaks suitable for developing a single multiple regression expression to predict concentration. Using SPSS (Statistical Package for the Social Sciences), a series of step-wise linear multiple regressions were run to search for correlations between elemental concentration (using one element at a time as the dependent variable) and binned peak areas (again using a running sum of five adjacent 0.1 nm) as the independent variables. In this technique, each independent variable is entered into the regression in order, beginning from the lowest wavelength bin, and then the R^2 value is calculated. All the R^2 values for a one-bin model are compared, and the single bin that best predicts concentration is chosen, as described by an equation of the form $Y = b_0 + b_1X_1$, where Y is the atomic fraction of the element being considered, X_n is peak area, b_0 is the intercept, and b_n is a partial regression coefficient. The procedure then retains the first bin as X_1, but repeats the test by entering into the regression all the remaining independent variables (bins), again one at a time, to produce an expression of the form $Y = b_0 + b_1X_1 + b_2X_2 + \ldots + b_nX_n$. It is important to note that the effects of the model are subtracted at each step to eliminate multicollinearity. In other words, the primary bin selected is the one related to the element of interest, and subsequent bins that co-vary with it (i.e. those arising from lines of the same element) will not be selected by

the regression because their variance is already represented in the equation. As a result, secondary, tertiary, etc. bins should represent lines arising from other elements contributing to matrix effects. This capability should prove useful in identifying the chemical relationships that are causing matrix effects for each element.

We used the SPSS default criteria for removal ($F \geq 0.1$) and inclusion ($F \leq 0.05$), where F is the F statistic. This PASRA method differs from the PLS used by *Clegg et al.* (2008) because it uses selected peak areas rather than the intensities at every channel.

As the number of independent variables increases, by definition the R^2 value also improves. For each different element, a surprisingly small number of "predictors" (n, the number of wavelength bins) was needed to achieve an R^2 value of 0.9995, which was arbitrarily chosen to represent a satisfactory fit. This number varied from 4 to 13 predictor bins per element over the range of each spectrometer. For this paper, which is intended to demonstrate proof-of-concept, only results for the visible wavelength range are shown; the analogous analysis can be done with UV or VNIR spectra as well, or the three ranges can be grouped together into a single file. The larger the range of wavelengths, the better the results will be because more and better diagnostic peaks for each element will be selected. Figure 1 (middle) shows the multiple regression results based on use of ten peak centroids for Ca. A nearly identical plot (with $R^2 >$ 0.9995 in all cases) could be shown for all the other major and minor elements listed in Table 1. It is apparent that the expression accurately predicts the concentration of the standards. Note also that its Y-intercept is almost exactly zero, suggesting that the expression is quite robust and free of matrix effects.

4. Validation

Validation tests were conducted for Ca as a test case using the running summed, 0.1 nm-binned data sets, both for 2048 channels in the VIS data alone, and for 6144 channels in the UV-VIS-NIR data set. One by one, each of the 21 spectra was removed from the data set, and the remaining 20 spectra were used to predict the composition of the 21st sample. Comparison of the results shows that although the first bin selected for all regressions is usually either 422.8 or 396.6 nm (both known Ca peaks), the subsequent bins chosen vary greatly according to which sample was excluded, with greater variation in bin choice when the larger wavelength range is considered. These validation results are unsurprising because the number of samples (n) in our data set is relatively small (only 21 "cases") and so the choice of bins is greatly biased by the removal of any individual sample. For these reasons, the R^2 values for a comparison of predicted vs. analyzed (by XRF) atomic fractions for Ca are only 0.66 for the VIS data alone and 0.58 for the entire wavelength range (Figure 1C). We anticipate that the validation plot R^2 values will improve when the number of samples in the calibration suite (as well as its chemical diversity), is larger. Increases in n should force the regression to generalize the non-primary bins that are common to all samples, and lessen the influence of any individual sample; work is in progress to test this hypothesis. For this technique to work effectively, it is apparent that we will need both a large number of samples and a wide range of concentrations in the calibration data sets for the Mars Science Laboratory.

5. Summary and Implications

For this size data set, the PLS analysis approach of *Clegg et al.* (2008) produces a far-superior ($R^2 = 0.987$) validation plot to the PASRA method, but for a logical reason: it uses variations in 6144 channels to predict concentration, compared with the 5-12 bins used by PASRA. The PLS approach also has the advantage of being completely without assumptions

regarding channel statistical selection and peak shape. PASRA is like PLS in that it can be directly tied to specific peaks known to be related to the elements of interest. However, PASRA is more easily understood from a traditional analytical chemistry viewpoint because it is based on peak areas rather than line intensities. Eventually, it may allow us to gain an understanding of which elements contribute to the matrix effects for which other elements, and why. Furthermore, the PASRA method, once fully calibrated, will be far less computationally intensive than the PLS techniques.

The PASRA has also been employed to quantify the minor and trace elements in these samples and the results shown in Table 1 are very encouraging (e.g., Zr plot in Figure 3). ChemCam will be the only instrument on Mars Science Laboratory capable of producing *quantitative* analyses of light minor elements like H, C, B, Li, O, and N. The lines from these elements are apparent in LIBS spectra of our volcanic rocks, even at very low concentrations, particularly for Li. It will be critical to ensure that appropriate calibration standards for those elements are also included in suites of laboratory standards.

It is likely that successful quantification of LIBS data for ChemCam will result from some combination of the two approaches. Future work will compare the two methods on a broader range of rock types and elemental concentrations, and explore other multivariate methods for selecting which peak areas/centroids lead to optimal quantitative analyses. It is already clear that considerable additional work is needed to develop large, well-characterized sample suites for laboratory calibration and validation, and to relate spectra of those suites to the calibration standards on the rover.

For the LIBS technique in laboratory applications, this analysis shows great promise. Future testing will examine the precision and accuracy of H, O, B, Be, Li, C, N, and other light elements under laboratory conditions using standards with known elemental concentrations (e.g., samples described in *McGuire et al.*,1992; *Dyar et al.*, 2002). Because LIBS can be done at microscopic scales, the technique may eventually offer the capability of quantitative microanalysis in many diverse types of materials.

Acknowledgments. This work was supported by NASA grant NNG06GH35G. We thank Mark Rivers for the use of his IDL routines, and Tony Lanzirotti for his help with their implementation.

References

Anzano, J.M., M.A. Villoria, A. Ruíz-Medina, and R.J. Lasheras (2006), Laser-induced breakdown spectroscopy for quantitative spectrochemical analysis of geological materials: Effects of the matrix and simultaneously determination, *Anal. Chim. Acta, 575*, 230-235.

Bousquet, B., J.-B. Sirven, and L. Canioni (2007), Towards quantitative laser-induced breakdown spectroscopy analysis of soil samples, *Spectroch. Acta B. Atom. Spectr., 62*, 1582-1589.

Buckley, S.G., H.A. Johnsen, K.R. Hencken, and D.W. Hahn (2000), Implementation of laser-induced breakdown spectroscopy as a continuous emissions monitor for toxic metals, *Waste Management, 20*, 455-462.

Clegg, S.A., R.C. Wiens, J. Barefield, E.C. Sklute, and M.D. Dyar (2008), Quantitative remote laser-Induced breakdown spectroscopy by multivariate analysis., *Spectroch. Acta B. Atom. Spectr.*, in press.

263 Dyar, M.D., M. Wiedenbeck, J.D. Robertson, L.R. Cross, J.S. Delaney, K. Ferguson, C.A.
264 Francis, E.S. Grew, C.V. Guidotti, R.L. Hervig, J.M. Hughes, J. Husler, W. Leeman, A.V.
265 McGuire, D. Rhede, H. Rothe, R.L. Paul., I. Richards, and M. Yates (2002), Reference
266 minerals for microanalysis of light elements, *Geostand. Newslet.*, *25*, 441-463.
267 Fabre, C., M.-C. Boiron, J. Dubessy, A. Chabiron, B. Charoy, and T.M. Crespo (2002),
268 Advances in lithium analysis in solids by means of laser-induced breakdown
269 spectroscopy : An exploratory study, *Geochim. Cosmochim. Acta*, *66*, 1401-1407.
270 Fink, H., Panne, U., and Neissner, R. (2002) Process analysis of recycled thermoplasts from
271 consumer electronics by laser-induced plasma spectroscopy. *Anal. Chem.*, *74*, 4334-4342.
272 Kajfosz, J., and W.M. Kwiatek (1987), Nonpolynomial approximation of background in x-ray-
273 spectra, *Nucl. Instr. Methods, B22*, 78-81.
274 Laville, S., M. Sabsabi, and F.R. Doucet (2007), Multi-elemental analysis of solidified mineral
275 melt samples by Laser-Induced Breakdown Spectroscopy coupled with a linear
276 multivariate calibration. *Spectroch. Acta B. Atom. Spectr.*, *62*, 1557-1566.
277 Le Bas, M.J and A.L. Streckeisen (1991) The IUGS systematics of igneous rocks, *J. Geol. Soc.*
278 *London*, *148*, 825-833.
279 Martin, M.Z., Labbé, N., Rials, T.G., and Wullschleger, S.D. (2005), Analysis of preservative-
280 treated wood by multivariate analysis of laser-induced breakdown spectroscopy spectra.
281 *Spectromchim. Acta*, 60, 1179-1185.
282 Maurice, S., R.C. Wiens, M. Saccoccio, B. Barraclough, B. Sallé, S.M. Clegg, and the
283 ChemCam team (2007), Expected performances of the ChemCam instrument for the
284 Mars Science Laboratory (MSL) rover. *Lunar Planet. Sci. XXXVIII.*, CD-ROM #1563
285 (abstr.).
286 McGuire, A.V., C.A. Francis, and M.D. Dyar (1992), Mineral standards for electron microprobe
287 analysis of oxygen, *Amer. Mineral.*, *77*, 1087-1091.
288 Palanco, S., and J.J. Laserna (2000), Full automation of a laser-induced breakdown spectrometer
289 for quality assessment in the steel industry with sample handling, surface preparation, and
290 quantitative analysis capabilities, *J. Anal. Atom. Spectrom.*, *15*, 1321-1327.
291 Rhodes, J.M., and M.J. Vollinger (2004) Composition of basaltic lavas sampled by phase-2 of
292 the Hawaii Scientific Drilling Project: Geochemical stratigraphy and magma types,
293 *Geochem., Geophys. Geosys.*, *5*, Q03G13.
294 Thompson, J.R., R.C. Wiens, J.E. Barefield, D.T. Vaniman, H.E. Newsom, and S.M. Clegg
295 (2006), *J. Geophys. Res.-Planets*, *111*, E05006.
296 Wiens, R.C., S. Maurice, S. Clegg, D. Vaniman, J. Thompson, M.D. Dyar, E.C. Sklute, H.
297 Newsom, N. Lanza, V. Sautter, J. Dubessy, J.-L. Lacour, B. Sallé, P. Mauchien, D.
298 Blaney, Y. Langevin, K. Herkenhoff, N. Bridges, G. Manhes, and the ChemCam team
299 (2007), Preparation of onboard calibration targets for the ChemCam instruments on the
300 Mars Science Laboratory rover, *Lunar Planet. Sci. XXXVIII.*, CD-ROM #1180 (abstr.).
301

302 Table 1. Compositional Ranges for Major and Minor Elements*

Species	Minimum	Maximum
Wt% SiO_2	43.29	76.58
Wt% TiO_2	0.09	6.22
Wt% Al_2O_3	4.04	17.46
Wt% Fe_2O_3	1.36	20.24
Wt% MnO	0.02	0.36
Wt% MgO	0.14	29.23
Wt% CaO	0.15	9.89
Wt% Na_2O	0.85	5.91
Wt% K_2O	0.39	5.60
Wt% P_2O_5	0.02	1.36
Ba, ppm	37	2980
Ce, ppm	10	195
Cr, ppm	4	1891
Ga, ppm	5	25
La, ppm	4	84
Nb, ppm	1.5	60.9
Ni, ppm	0	1183
Pb, ppm	2	40
Rb, ppm	3.7	223
Sr, ppm	16	819
Th, ppm	1	22
U, ppm	0	5
V, ppm	2	374
Y, ppm	2.4	82.5
Zn, ppm	27	272
Zr, ppm	41	914

303 *Values determined by XRF, given in wt. % oxide or ppm as noted. Total iron is calculated as Fe_2O_3.
304

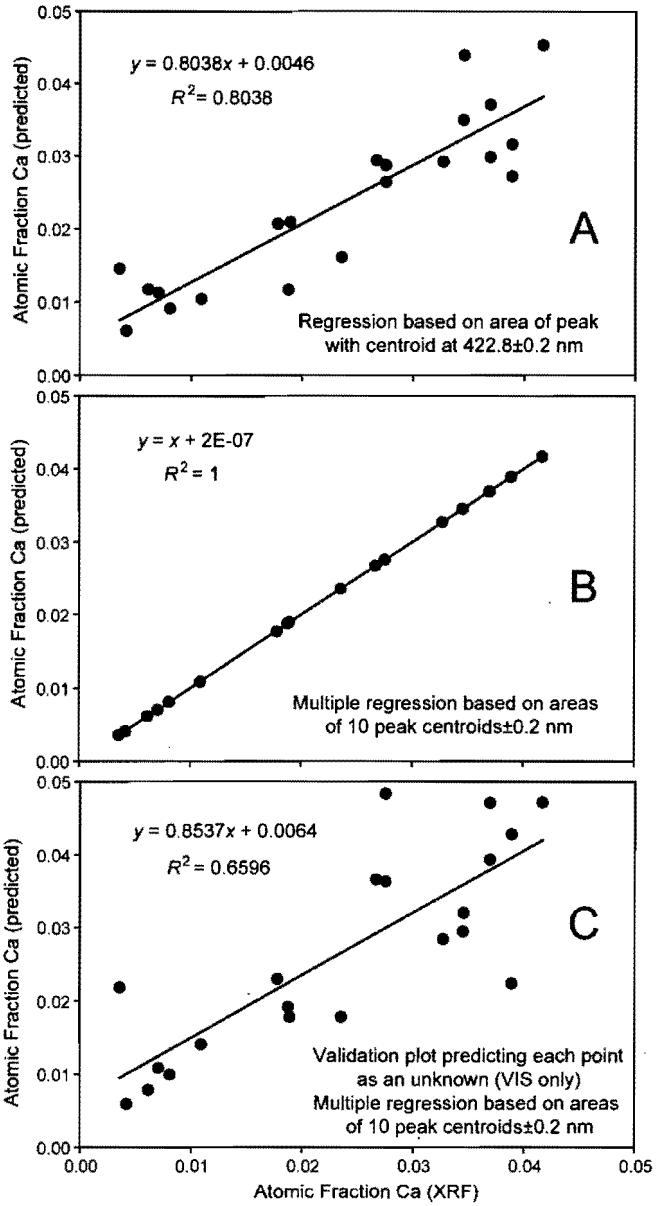

Figure 1. **A.** Single linear regression using the summed areas of the five 0.1 nm bins centered on 422.8 nm for all 21 samples; the *x* axis shows the atomic fraction of Ca measured by XRF, and the *y* axis shows the predicted atomic fraction. The non-zero intercept on the *y* axis implies that some other element is affecting these peak areas. **B.** Multiple regression analysis using summed areas of the five 0.1 nm bins centered on each of ten centroids; the actual R^2 value is 0.9996. Axes as in A. Note that the intercept is very close to zero, suggesting that this method compensates for matrix effects successfully. **C.** Validation plot using visible wavelength data only. One sample at a time was removed for the data set before a multiple regression expression was calculated and then used to predict the composition of that sample. Axes as in A. As the number of samples and the chemical diversity represented in the calibration suite is increased (through work in progress), this correlation should become increasingly better. This plot underscores the importance of developing predictive equations based on calibration data sets with as much depth and breadth as possible.

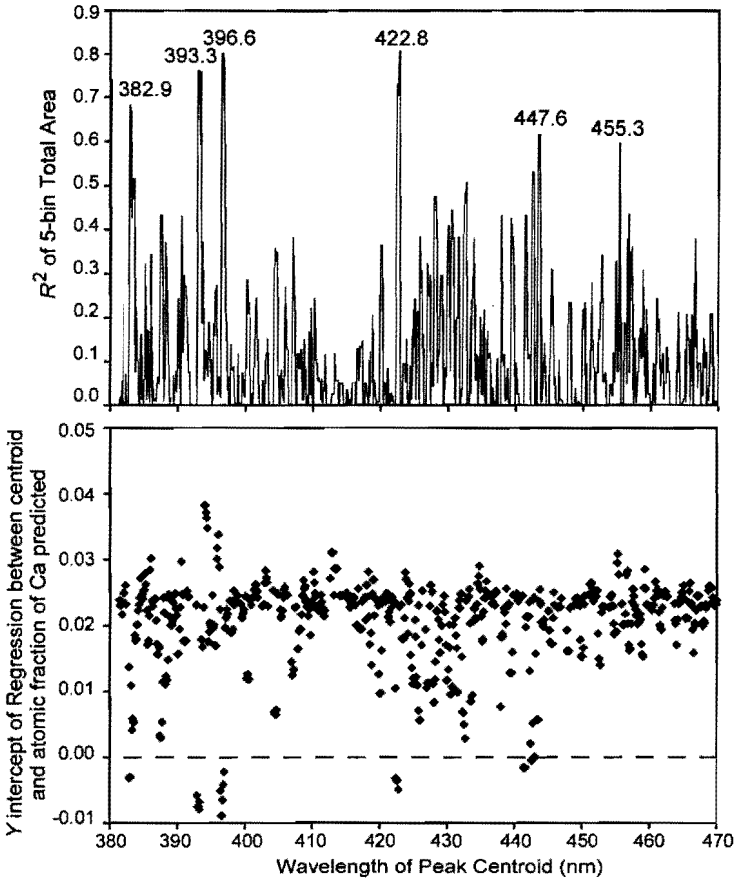

Figure 2. Graphs showing where there are correlations between the atomic fraction of Ca and the area of peaks centered at each wavelength measured. Top: R^2 values for the summed peak areas of five adjacent 0.1 nm bins regressed against the atomic fraction of Ca. Note that the areas of the prominent peaks at 393.3 and 396.6 nm, commonly used for Ca determinations elsewhere in the literature, do correlate well with Ca; the best correlation is at 422.8 nm. Bottom: *Y* intercept values for the regressions shown in A, plotted against the wavelength of the bin centroid.

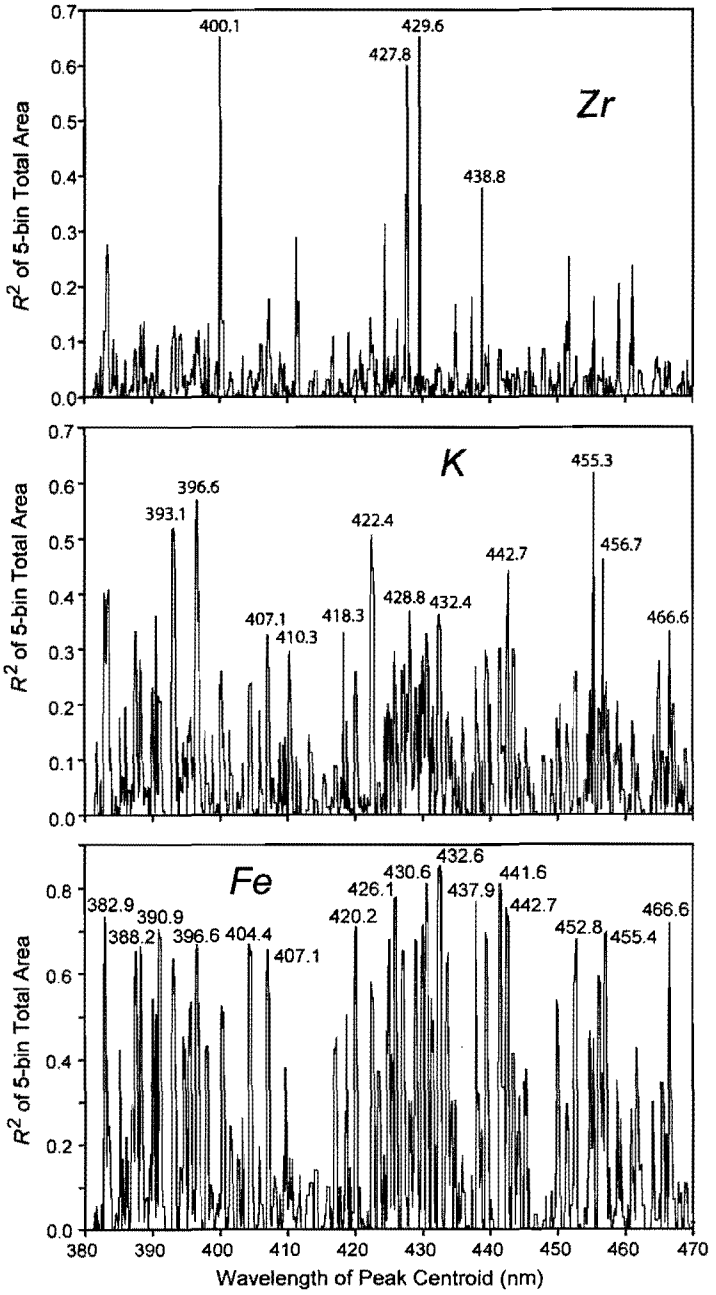

331
332

333 Figure 3. R^2 values (y axis) for the summed peak areas of five adjacent 0.1 nm bins regressed
334 against the atomic fractions of Zr (top), K (middle) and Fe (bottom) as a function of wavelength.
335 Note that some of the observed peaks with high correlations may be due to emissions from
336 compatible elements.